Search for astrophysical tau neutrinos in three years of IceCube data

M. G. Aartsen,[2] K. Abraham,[32] M. Ackermann,[48] J. Adams,[15] J. A. Aguilar,[12] M. Ahlers,[29] M. Ahrens,[39] D. Altmann,[23] T. Anderson,[45] I. Ansseau,[12] M. Archinger,[30] C. Arguelles,[29] T. C. Arlen,[45] J. Auffenberg,[1] X. Bai,[37] S. W. Barwick,[26] V. Baum,[30] R. Bay,[7] J. J. Beatty,[17,18] J. Becker Tjus,[10] K.-H. Becker,[47] E. Beiser,[29] S. BenZvi,[29] P. Berghaus,[48] D. Berley,[16] E. Bernardini,[48] A. Bernhard,[32] D. Z. Besson,[27] G. Binder,[8,7] D. Bindig,[47] M. Bissok,[1] E. Blaufuss,[16] J. Blumenthal,[1] D. J. Boersma,[46] C. Bohm,[39] M. Börner,[20] F. Bos,[10] D. Bose,[41] S. Böser,[30] O. Botner,[46] J. Braun,[29] L. Brayeur,[13] H.-P. Bretz,[48] N. Buzinsky,[22] J. Casey,[5] M. Casier,[13] E. Cheung,[16] D. Chirkin,[29] A. Christov,[24] K. Clark,[42] L. Classen,[23] S. Coenders,[32] D. F. Cowen,[45,44] A. H. Cruz Silva,[48] J. Daughhetee,[5] J. C. Davis,[17] M. Day,[29] J. P. A. M. de André,[21] C. De Clercq,[13] E. del Pino Rosendo,[30] H. Dembinski,[33] S. De Ridder,[25] P. Desiati,[29] K. D. de Vries,[13] G. de Wasseige,[13] M. de With,[9] T. DeYoung,[21] J. C. Díaz-Vélez,[29] V. di Lorenzo,[30] J. P. Dumm,[39] M. Dunkman,[45] R. Eagan,[45] B. Eberhardt,[30] T. Ehrhardt,[30] B. Eichmann,[10] S. Euler,[46] P. A. Evenson,[33] O. Fadiran,[29] S. Fahey,[29] A. R. Fazely,[6] A. Fedynitch,[10] J. Feintzeig,[29] J. Felde,[16] K. Filimonov,[7] C. Finley,[39] T. Fischer-Wasels,[47] S. Flis,[39] C.-C. Fösig,[30] T. Fuchs,[20] T. K. Gaisser,[33] R. Gaior,[14] J. Gallagher,[28] L. Gerhardt,[8,7] K. Ghorbani,[29] D. Gier,[1] L. Gladstone,[29] M. Glagla,[1] T. Glüsenkamp,[48] A. Goldschmidt,[8] G. Golup,[13] J. G. Gonzalez,[33] D. Góra,[48] D. Grant,[22] J. C. Groh,[45] A. Groß,[32] C. Ha,[8,7] C. Haack,[1] A. Haj Ismail,[25] A. Hallgren,[46] F. Halzen,[29] E. Hansen,[19] B. Hansmann,[1] K. Hanson,[29] D. Hebecker,[9] D. Heereman,[12] K. Helbing,[47] R. Hellauer,[16] S. Hickford,[47] J. Hignight,[21] G. C. Hill,[2] K. D. Hoffman,[16] R. Hoffmann,[47] K. Holzapfel,[32] A. Homeier,[11] K. Hoshina,[29,*] F. Huang,[45] M. Huber,[32] W. Huelsnitz,[16] P. O. Hulth,[39] K. Hultqvist,[39] S. In,[41] A. Ishihara,[14] E. Jacobi,[48] G. S. Japaridze,[4] K. Jero,[29] M. Jurkovic,[32] A. Kappes,[23] T. Karg,[48] A. Karle,[29] M. Kauer,[29,34] A. Keivani,[45] J. L. Kelley,[29] J. Kemp,[1] A. Kheirandish,[29] J. Kiryluk,[40] J. Kläs,[47] S. R. Klein,[8,7] G. Kohnen,[31] R. Koirala,[33] H. Kolanoski,[9] R. Konietz,[1] L. Köpke,[30] C. Kopper,[22] S. Kopper,[47] D. J. Koskinen,[19] M. Kowalski,[9,48] K. Krings,[32] G. Kroll,[30] M. Kroll,[10] J. Kunnen,[13] N. Kurahashi,[36] T. Kuwabara,[14] M. Labare,[25] J. L. Lanfranchi,[45] M. J. Larson,[19] M. Lesiak-Bzdak,[40] M. Leuermann,[1] J. Leuner,[1] L. Lu,[14] J. Lünemann,[13] J. Madsen,[38] G. Maggi,[13] K. B. M. Mahn,[21] R. Maruyama,[34] K. Mase,[14] H. S. Matis,[8] R. Maunu,[16] F. McNally,[29] K. Meagher,[12] M. Medici,[19] A. Meli,[25] T. Menne,[20] G. Merino,[29] T. Meures,[12] S. Miarecki,[8,7] E. Middell,[48] E. Middlemas,[29] L. Mohrmann,[48] T. Montaruli,[24] R. Morse,[29] R. Nahnhauer,[48] U. Naumann,[47] G. Neer,[21] H. Niederhausen,[40] S. C. Nowicki,[22] D. R. Nygren,[8] A. Obertacke,[47] A. Olivas,[16] A. Omairat,[47] A. O'Murchadha,[12] T. Palczewski,[43] H. Pandya,[33] D. V. Pankova,[45] L. Paul,[1] J. A. Pepper,[43] C. Pérez de los Heros,[46] C. Pfendner,[17] D. Pieloth,[20] E. Pinat,[12] J. Posselt,[47] P. B. Price,[7] G. T. Przybylski,[8] J. Pütz,[1] M. Quinnan,[45] C. Raab,[12] L. Rädel,[1] M. Rameez,[24] K. Rawlins,[3] R. Reimann,[1] M. Relich,[14] E. Resconi,[32] W. Rhode,[20] M. Richman,[36] S. Richter,[29] B. Riedel,[22] S. Robertson,[2] M. Rongen,[1] C. Rott,[41] T. Ruhe,[20] D. Ryckbosch,[25] S. M. Saba,[10] L. Sabbatini,[29] H.-G. Sander,[30] A. Sandrock,[20] J. Sandroos,[30] S. Sarkar,[19,35] K. Schatto,[30] F. Scheriau,[20] M. Schimp,[1] T. Schmidt,[16] M. Schmitz,[20] S. Schoenen,[1] S. Schöneberg,[10] A. Schönwald,[48] L. Schulte,[11] D. Seckel,[33] S. Seunarine,[38] M. W. E. Smith,[45] D. Soldin,[47] M. Song,[16] G. M. Spiczak,[38] C. Spiering,[48] M. Stahlberg,[1] M. Stamatikos,[17,†] T. Stanev,[33] N. A. Stanisha,[45] A. Stasik,[48] T. Stezelberger,[8] R. G. Stokstad,[8] A. Stößl,[48] R. Ström,[46] N. L. Strotjohann,[48] G. W. Sullivan,[16] M. Sutherland,[17] H. Taavola,[46] I. Taboada,[5] J. Tatar,[8,7] S. Ter-Antonyan,[6] A. Terliuk,[48] G. Tešić,[45] S. Tilav,[33] P. A. Toale,[43] M. N. Tobin,[29] S. Toscano,[13] D. Tosi,[29] M. Tselengidou,[23] A. Turcati,[32] E. Unger,[46] M. Usner,[48] S. Vallecorsa,[24] J. Vandenbroucke,[29] N. van Eijndhoven,[13] S. Vanheule,[25] J. van Santen,[48] J. Veenkamp,[32] M. Vehring,[1] M. Voge,[11] M. Vraeghe,[25] C. Walck,[39] A. Wallace,[2] M. Wallraff,[1] N. Wandkowsky,[29] Ch. Weaver,[22] C. Wendt,[29] S. Westerhoff,[29] B. J. Whelan,[2] N. Whitehorn,[29] K. Wiebe,[30] C. H. Wiebusch,[1] L. Wille,[29] D. R. Williams,[43,‡] H. Wissing,[16] M. Wolf,[39] T. R. Wood,[22] K. Woschnagg,[7] D. L. Xu,[43,§] X. W. Xu,[6] Y. Xu,[40] J. P. Yanez,[48] G. Yodh,[26] S. Yoshida,[14] and M. Zoll[39]

(IceCube Collaboration)

[1]*III. Physikalisches Institut, RWTH Aachen University, D-52056 Aachen, Germany*
[2]*Department of Physics, University of Adelaide, Adelaide 5005, Australia*
[3]*Department of Physics and Astronomy, University of Alaska Anchorage, 3211 Providence Dr., Anchorage, Alaska 99508, USA*
[4]*CTSPS, Clark-Atlanta University, Atlanta, Georgia 30314, USA*
[5]*School of Physics and Center for Relativistic Astrophysics, Georgia Institute of Technology, Atlanta, Georgia 30332, USA*
[6]*Department of Physics, Southern University, Baton Rouge, Louisiana 70813, USA*
[7]*Department of Physics, University of California, Berkeley, California 94720, USA*
[8]*Lawrence Berkeley National Laboratory, Berkeley, California 94720, USA*
[9]*Institut für Physik, Humboldt-Universität zu Berlin, D-12489 Berlin, Germany*
[10]*Fakultät für Physik & Astronomie, Ruhr-Universität Bochum, D-44780 Bochum, Germany*
[11]*Physikalisches Institut, Universität Bonn, Nussallee 12, D-53115 Bonn, Germany*

[12]*Université Libre de Bruxelles, Science Faculty CP230, B-1050 Brussels, Belgium*
[13]*Vrije Universiteit Brussel, Dienst ELEM, B-1050 Brussels, Belgium*
[14]*Department of Physics, Chiba University, Chiba 263-8522, Japan*
[15]*Department of Physics and Astronomy, University of Canterbury, Private Bag 4800 Christchurch, New Zealand*
[16]*Department of Physics, University of Maryland, College Park, Maryland 20742, USA*
[17]*Department of Physics and Center for Cosmology and Astro-Particle Physics, Ohio State University, Columbus, Ohio 43210, USA*
[18]*Department of Astronomy, Ohio State University, Columbus, Ohio 43210, USA*
[19]*Niels Bohr Institute, University of Copenhagen, DK-2100 Copenhagen, Denmark*
[20]*Department of Physics, TU Dortmund University, D-44221 Dortmund, Germany*
[21]*Department of Physics and Astronomy, Michigan State University, East Lansing, Michigan 48824, USA*
[22]*Department of Physics, University of Alberta, Edmonton, Alberta, Canada T6G 2E1*
[23]*Erlangen Centre for Astroparticle Physics, Friedrich-Alexander-Universität Erlangen-Nürnberg, D-91058 Erlangen, Germany*
[24]*Département de physique nucléaire et corpusculaire, Université de Genève, CH-1211 Genève, Switzerland*
[25]*Department of Physics and Astronomy, University of Gent, B-9000 Gent, Belgium*
[26]*Department of Physics and Astronomy, University of California, Irvine, California 92697, USA*
[27]*Department of Physics and Astronomy, University of Kansas, Lawrence, Kansas 66045, USA*
[28]*Department of Astronomy, University of Wisconsin, Madison, Wisconsin 53706, USA*
[29]*Department of Physics and Wisconsin IceCube Particle Astrophysics Center, University of Wisconsin, Madison, Wisconsin 53706, USA*
[30]*Institute of Physics, University of Mainz, Staudinger Weg 7, D-55099 Mainz, Germany*
[31]*Université de Mons, 7000 Mons, Belgium*
[32]*Technische Universität München, D-85748 Garching, Germany*
[33]*Bartol Research Institute and Department of Physics and Astronomy, University of Delaware, Newark, Delaware 19716, USA*
[34]*Department of Physics, Yale University, New Haven, Connecticut 06520, USA*
[35]*Department of Physics, University of Oxford, 1 Keble Road, Oxford OX1 3NP, United Kingdom*
[36]*Department of Physics, Drexel University, 3141 Chestnut Street, Philadelphia, Pennsylvania 19104, USA*
[37]*Physics Department, South Dakota School of Mines and Technology, Rapid City, South Dakota 57701, USA*
[38]*Department of Physics, University of Wisconsin, River Falls, Wisconsin 54022, USA*
[39]*Oskar Klein Centre and Department of Physics, Stockholm University, SE-10691 Stockholm, Sweden*
[40]*Department of Physics and Astronomy, Stony Brook University, Stony Brook, New York 11794-3800, USA*
[41]*Department of Physics, Sungkyunkwan University, Suwon 440-746, Korea*
[42]*Department of Physics, University of Toronto, Toronto, Ontario, Canada, M5S 1A7*
[43]*Department of Physics and Astronomy, University of Alabama, Tuscaloosa, Alabama 35487, USA*
[44]*Department of Astronomy and Astrophysics, Pennsylvania State University, University Park, Pennsylvania 16802, USA*
[45]*Department of Physics, Pennsylvania State University, University Park, Pennsylvania 16802, USA*
[46]*Department of Physics and Astronomy, Uppsala University, Box 516, S-75120 Uppsala, Sweden*
[47]*Department of Physics, University of Wuppertal, D-42119 Wuppertal, Germany*
[48]*DESY, D-15735 Zeuthen, Germany*

(Received 22 September 2015; published 12 January 2016)

The IceCube Neutrino Observatory has observed a diffuse flux of TeV-PeV astrophysical neutrinos at 5.7σ significance from an all-flavor search. The direct detection of tau neutrinos in this flux has yet to occur. Tau neutrinos become distinguishable from other flavors in IceCube at energies above a few hundred TeV, when the cascade from the tau neutrino charged current interaction becomes resolvable from the cascade from the

[*]Also at Earthquake Research Institute, University of Tokyo, Bunkyo, Tokyo 113-0032, Japan.
[†]Also at NASA Goddard Space Flight Center, Greenbelt, MD 20771, USA.
[‡]Corresponding author.
drwilliams3@ua.edu
[§]Corresponding author.
dxu@icecube.wisc.edu

tau lepton decay. This paper presents results from the first dedicated search for tau neutrinos with energies between 214 TeV and 72 PeV in the full IceCube detector. The analysis searches for IceCube optical sensors that observe two separate pulses in a single event—one from the tau neutrino interaction and a second from the tau decay. No candidate events were observed in three years of IceCube data. For the first time, a differential upper limit on astrophysical tau neutrinos is derived around the PeV energy region, which is nearly 3 orders of magnitude lower in energy than previous limits from dedicated tau neutrino searches.

DOI: 10.1103/PhysRevD.93.022001

I. INTRODUCTION

The IceCube Neutrino observatory has announced a significant detection of a diffuse astrophysical neutrino flux above 30 TeV [1,2]. The source of this flux is as yet unknown, with possible candidates including cosmic ray acceleration in active galactic nuclei, gamma ray bursts, and supernova remnants. Assuming standard 3-flavor oscillations and a most commonly considered $\nu_e : \nu_\mu : \nu_\tau = 1 : 2 : 0$ flux from pion decay at the source, the neutrinos detected in IceCube should be divided almost equally into all three flavors [3]. Other flavor compositions at the source ranging from 1: 0: 0 to 0: 1: 0 are possible for dominant processes such as neutron decay [4], energy loss of pions and muons before decay in an environment with strong magnetic fields or high matter density [5–8], and muon acceleration [9]. Though those scenarios result in nonuniversal flavor ratios at Earth, they all predict significant fluxes of tau neutrinos after averaged oscillations by propagation over astronomical distances [10–12]. Above PeV energies, the Earth becomes opaque to electron and muon neutrinos, while the tau neutrino flux is regenerated through subsequent tau lepton decays to neutrinos [13]. Tau neutrino background from the atmosphere is expected to be negligible at high energies, with only a small contribution from the decay of charmed mesons [14]. Therefore the detection of tau neutrinos at high energies would both give new information about the astrophysical flux as well as serving as an additional confirmation of the astrophysical origin of the high energy diffuse neutrino signal. Two recent flavor ratio analyses of IceCube high energy neutrino events were consistent with equal fractions of all flavors in IceCube, though with large uncertainty [11,12]. Neither flavor ratio analysis included a dedicated tau neutrino identification algorithm, which would improve the measurement of astrophysical neutrino flavor ratios. Precise measurement of astrophysical neutrino flavor content at Earth will shed light on the emission mechanisms at the source, test the fundamental properties of neutrinos over extremely long baselines and better constrain new physics models which predict significant deviations from equal fractions of all flavors [15–24].

Most neutrino interactions in IceCube have one of two event topologies: tracks from charged current (CC) interactions of muon neutrinos, and cascades (or showers) from CC interactions of electron and low energy tau neutrinos and neutral current (NC) interactions of all flavors. As the average tau decay length roughly scales as 5 cm/TeV, at energies above a few hundred TeV, the tau lepton produced in a tau neutrino CC interaction would have a decay length sufficiently long that the CC interaction of the tau neutrino and the subsequent decay of the tau lepton could be resolved by IceCube sensors. There is an 83% chance that the tau lepton decays to electrons or hadrons, producing a second cascade. This double cascade signal is called a "double bang" [3]; an event sketch is shown in Fig. 1.

A previous IceCube search for high energy tau neutrinos was published using data from the partially completed detector [25]. Since a fully contained double bang is unlikely to be contained in the small size of the incomplete detector, the search was optimized for partially contained double bangs. The search led to a null result and was in fact more sensitive to electron and muon flavor neutrinos than to tau neutrinos.

There is a 17% chance of the tau decaying to a muon, producing an outgoing track. Therefore, another possible search method is to look for a track that abruptly brightens along its length as the muon produces light more efficiently than the parent tau [26]. Tau neutrinos may also produce a signature in cosmic ray air shower detectors. The Pierre Auger Observatory has reported an upper limit on the tau neutrino flux from a search for horizontal showers from tau lepton decays induced by Earth-skimming cosmogenic neutrinos. However, the energy threshold of this search is 200 PeV, much higher than the energy of the astrophysical neutrinos observed by IceCube [27].

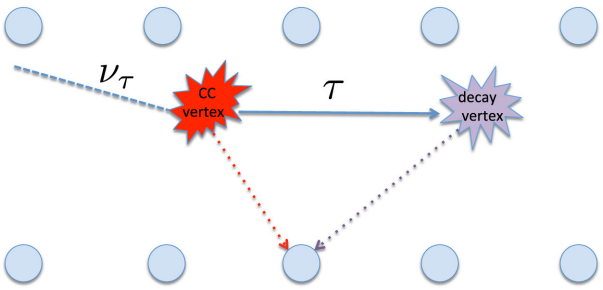

FIG. 1. Sketch of a ν_τ undergoing a charged current interaction and producing a double bang signature in IceCube. The blue circles represent IceCube photon sensors buried in the ice. This figure is not drawn to scale.

This paper describes a new search method for double bangs whose two cascades may not be separately reconstructed, but which appear as a two-peaked or "double pulse" waveform in one or more IceCube sensors.

II. THE ICECUBE DETECTOR

The IceCube detector [28] consists of 86 vertical cables, called strings, deployed in the ice near the geographic South Pole. Each string contains 60 digital optical modules (DOMs). A DOM consists of a ten-inch photomultiplier tube (PMT), digitizing electronics, and LED flashers for calibration [29]. The digitized PMT signal is called a waveform. The DOM utilizes two digitizers: the analog transient waveform digitizer (ATWD) which digitizes at 3.3 ns per sample for 128 samples, and the fast analog-to-digital converter (fADC) which digitizes continuously at 25 ns per sample, with a record length set at 256 samples. The ATWD output is separated into three different gain channels (x16, x2, x0.25) to cover the dynamic range of the PMT, which has a linear response (within 10%) up to currents of 400 photoelectrons (PE) per 15 ns [30]. When a PMT receives a signal above a threshold of 0.25 PE, this is called a hit. The x16 gain channel is captured first, with the x2 and x0.25 channels captured if the next lowest gain channel exceeds 768 ADC counts in any sample. A local coincidence hit (LC) occurs if a pair of nearest or next-to-nearest neighbor DOMs on the same string are hit within one microsecond. For LC hits, the complete ATWD and fADC waveforms will be sent to the surface. The primary IceCube trigger keeps all DOM hits if eight or more LC hits occur anywhere in the detector within a five-microsecond window; such a collection of DOM hits is called an event.

IceCube employs a number of filtering algorithms in order to reduce the data volume for transmission to the Northern hemisphere. The analysis described in this paper uses the "extremely high energy" (EHE) filtering algorithm, which keeps all events that deposit more than 1000 PE in the detector.

IceCube was fully built as of December 2010. This analysis uses 914.1 days of data from the full detector between May 13, 2011, and May 6, 2014. The data were kept in the analysis chain only when all IceCube strings were operating and no *in situ* calibration light sources were in use.

Background and signal passing rates were computed using Monte Carlo simulation. The CORSIKA [31] simulation package is used to generate cosmic-ray-induced muons. Astrophysical and atmospheric neutrinos are simulated using an adapted version of the Monte Carlo generator ANIS [32]. Photon propagation through the ice is simulated as described in [33]. PMT response and digitization electronics are fully simulated, which is particularly important for this analysis.

In addition to the simulation, 10% of the data were used to develop cuts and estimate cosmic ray muon background rates, with the rest of the data not used until the cuts were finalized.

III. SEARCH FOR TAU NEUTRINOS

A. Double pulse algorithm

The goal of the double pulse algorithm (DPA) is to identify double pulse waveforms that are consistent with ν_τ CC interaction signatures in IceCube, while rejecting waveforms with features that are consistent with late scattered photons from single cascade events from NC and ν_e CC interactions. There are two additional types of background events which could produce substantial double pulse waveforms: (1) high-energy single muons and/or muon bundles induced by cosmic rays interacting with the atmosphere and (2) ν_μ CC interactions in IceCube which produce energetic muons. For double pulse waveforms caused by energetic atmospheric muons, the first pulse is usually from a combination of Cherenkov light emissions and coincident stochastic energy loss, and the second pulse is from TeV-scale stochastic energy losses tens of meters away from the DOM. For double pulse waveforms from astrophysical ν_μ CC events, the first pulse is from energy deposition of the CC hadronic interaction vertex, while the second pulse is from a coincident stochastic energy loss of the energetic outgoing muon. Since the double pulse waveforms from ν_τ CC events, energetic atmospheric muons and astrophysical ν_μ CC events are not distinguishable from one another as they are caused by the same mechanism of two substantial energy depositions near certain DOMs, we do not remove these events with the DPA. They are to be removed later by comparing their overall topologies and timing profiles. The potential impact of instrumental backgrounds on the DPA was found to be negligible. Afterpulses in the PMT waveforms, caused by ionization of residual gases by electrons accelerated in the space between dynodes, usually occur from 500 ns to microseconds later than the primary pulse, and therefore do not appear as double pulses in a single waveform. Late pulses, caused by photoelectrons backscattered from the first dynode, occur on a time scale of 60 ns later than the primary pulse, but usually have a low amplitude and do not trigger the DPA [29].

The DPA uses the positive and negative first derivatives of a waveform to determine rising and trailing edges. A double pulse is defined as a rising edge, followed by a trailing edge, followed by another rising edge. Waveforms from the ATWD digitizer in the lowest gain channel available are used since higher gain channels are usually saturated for high amplitude waveforms. The fADC waveforms are not used since they do not have multiple gain channels available and since their coarser timing causes double pulse features to be blended together or saturated. The DPA uses the following seven configurable parameters to characterize a double pulse waveform:

(i) Since signal waveforms are from bright events close to a DOM, the DPA is only run on ATWD waveforms that have integrated charge greater than $q_1 = 432$ PE.

(ii) The beginning of the waveform is determined by a sliding time window of 3.3 ns which searches for a monotonic increase in the waveform amplitude within a time span of $3.3 \times 6 = 19.8$ ns.

(iii) Once the beginning of the waveform is identified, the waveform is divided into segments of four ATWD bins (13.2 ns) and the first derivative of the waveform is computed in each segment.

(iv) If the first derivative is positive in $n_1 = 2$ consecutive segments, this is considered the rising edge of the first pulse. When the subsequent derivative is negative for $n_2 = 2$ consecutive segments, this is considered the trailing edge of the first pulse. The rising edge of the first pulse is required to have an integrated charge of at least $q_2 = 23$ PE, and the integrated charge of the trailing edge is required to be at least $q_3 = 39$ PE. The integrated charge sums up all the charge corresponding to the entire rising or trailing edges, which usually last longer than two segments (26.4 ns) for a large pulse.

(v) The second pulse rising edge is defined when the derivative after the trailing edge of the first pulse is positive again for $n_3 = 3$ consecutive segments. This requirement is due to the fact that the light in the second pulse is often more scattered and therefore has a less steep rising edge than the first pulse. The second pulse trailing edge is often outside the ATWD window, and hence is not included in the calculation. The rising edge of the second pulse is required to have an integrated charge of at least $q_4 = 42$ PE.

The configurable DPA parameters n_i and q_i were tested and optimized using a variety of IceCube event waveforms including simulated neutrinos of all flavors, simulated atmospheric muons and data from *in situ* laser calibration devices. An example of a simulated double pulse waveform from a ν_τ CC event is shown in Fig. 2. The production of double pulse waveforms depends largely on the distances between event interaction vertices and nearby DOMs. The median distance between the ν_τ CC (tau lepton decay) vertices and the double pulse DOMs is 49 (44) meters.

The fraction of events that pass a charge cut of $\log_{10}(\mathrm{QTot}) > 3.3$ and have at least one double pulse waveform is shown in Fig. 3 as a function of deposited charge, for both the 10% data sample and atmospheric muon simulation. Near the charge cut threshold, fewer than 1 in 1000 events will include a double pulse waveform.

B. Event selection

The event selection process was carried out at three cut levels, driven by the specific goal of background rejection at each level. To conform with standard IceCube usage, the cuts for this analysis are numbered beginning with level 4. The cut levels are summarized as follows:

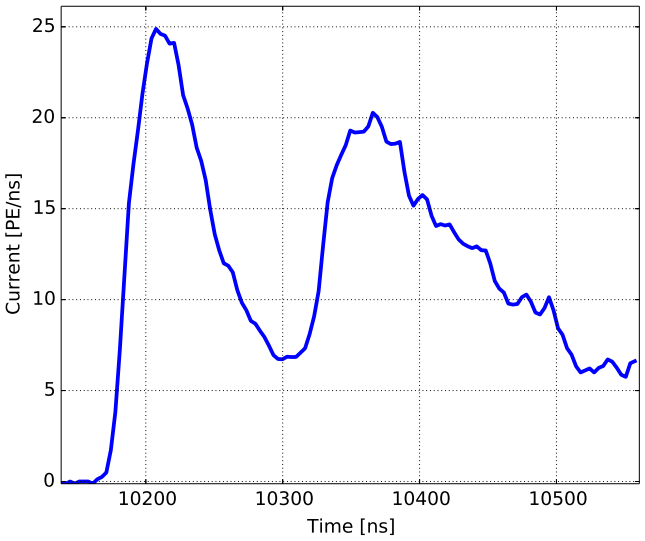

FIG. 2. A simulated double pulse waveform obtained in one DOM from a ν_τ CC event. The primary neutrino energy for this event is 2.4 PeV, about 75% of this energy transfers to the outgoing τ^- lepton, which travels 40 meters before decay. In this event, a total of 34 double pulse waveforms were produced from adjacent DOMs on neighboring strings near the event interaction vertices. The distances from the CC vertex and the τ^- decay vertex to the DOM that produced this double pulse waveform are 76 m and 75 m, respectively. Time = 0 corresponds to the beginning of the event readout window, which begins 10 microseconds before the event trigger launches.

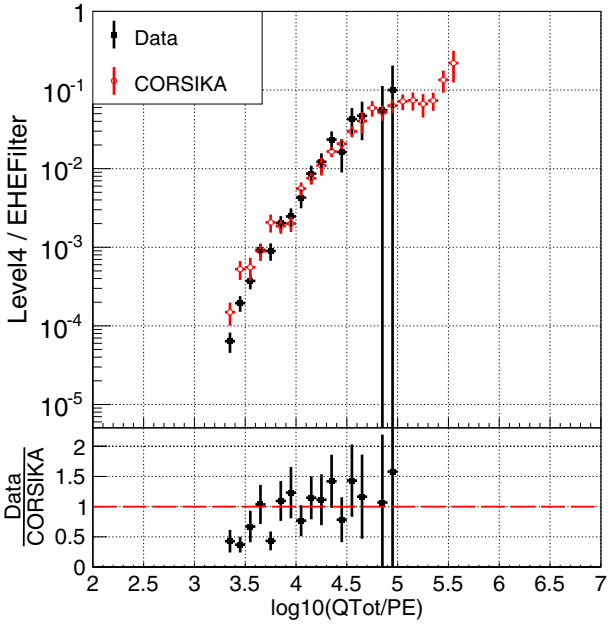

FIG. 3. Fraction of events that pass the charge cut of $\log_{10}(\mathrm{QTot}) > 3.3$ and have at least one double pulse waveform as a function of total deposited charge. The higher the charge in the event, the more likely it is to contain at least one double pulse waveform. Muons with lower deposited charge that might evade containment cuts are less likely to produce double pulse waveforms.

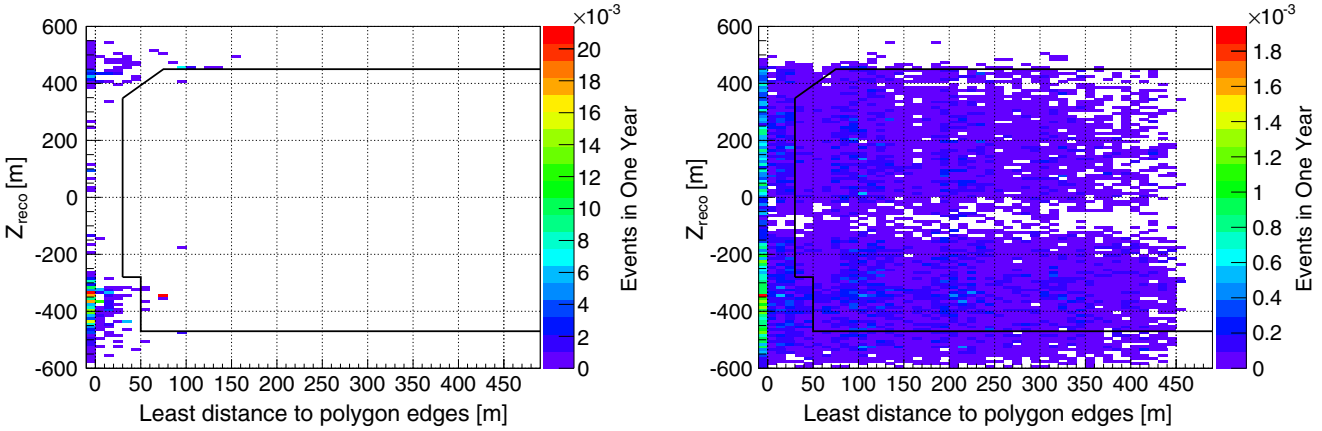

FIG. 4. Events per year that pass the level-6 containment cut on depth and distance to the detector edge (solid line) for simulated atmospheric muons (left) and astrophysical ν_τ (right).

Level 4: Events are required to have at least one waveform which passes the DPA. An additional event-wise charge cut of $\log_{10}(\mathrm{QTot}) > 3.3$ is also required to enrich the sample with high energy events.

Level 5: At this stage, we remove tracklike double pulse events which are predominantly due to atmospheric muons.

Following the level 4 cut, each event is reconstructed using a maximum likelihood method based on a hypothesis of an infinite track and a hypothesis of a pointlike cascade. These reconstructions only make use of the timing information for the earliest photon arriving at the DOMs and hence are computationally efficient. The reduced log likelihood ratio between the two hypotheses $L_R = \log(L_{\mathrm{cascade}}/L_{\mathrm{track}})$ is required to be negative, indicating the event topology is more cascadelike than tracklike. This cut eliminates most down-going energetic muons and muon bundles. To further veto down-going muons, the first hit in the event is required to be below the top 40 meters of the instrumented volume. CORSIKA simulation predicts that 3.5 ± 3.4 atmospheric muons survive to level 5 in 914.1 days.

Level 6: At this stage we eliminate cosmic-ray-induced muons which pass near the edges of the detector and, hence, appear cascadelike. An additional reconstruction algorithm is performed on all events which pass the preceding cuts, using full charge and time information, which is more computationally expensive. A boundary is defined by the surface connecting the position of the outermost layer of strings in the detector. The containment criterion requires that the reconstructed vertex be inside the instrumented volume and a given distance away from the boundary. The distance from the boundary depends on depth, with stricter containment required at the top and bottom of the detector. The containment is illustrated in Fig. 4, which shows the distribution of event vertices with respect to the boundary for signal and for atmospheric muon background. Due to the scarcity of events in the atmospheric muon simulation at high energies, the double pulse criterion is removed from this plot, with all other cuts kept. The very few atmospheric muon events which survive the containment cut are close to the charge cut threshold, and as shown in Fig. 3, such events have a lower probability of producing a double pulse waveform.

At the final cut level, the predicted rates from all sources in three years of data are summarized in Table I. The assumed astrophysical flux is based on the diffuse flux measured by IceCube at the level of $\mathrm{E}^2\Phi_\nu = 1.0 \times 10^{-8}$ GeV cm^{-2} s^{-1} sr^{-1} per flavor [2], and 90% of the predicted ν_τ CC events are between 214 TeV and 72 PeV. A softer neutrino energy spectrum of $\mathrm{E}^{-2.5}$ [12] reduces the expected number of ν_τ events and the dominant background of ν_μ CC events by 36% and 57% respectively. The atmospheric neutrino rate prediction includes both neutrinos from π/K decay [34] and neutrinos from charmed meson decay [14]. The primary cosmic ray spectrum used to predict atmospheric neutrino rates is corrected for air shower measurements in the knee region of several PeV [35].

Figure 5 summarizes the passing rate of signal and background events at each cut level. At the final cut level, astrophysical ν_τ events have the highest passing rate of any source, and the dominant background is astrophysical ν_μ CC events. The effective areas for ν_τ CC and ν_μ CC events at the final cut level is shown in Fig. 6. An optimal energy window for the astrophysical ν_τ search in IceCube using

TABLE I. Predicted event rates from all sources at the final cut level. Errors are statistical only.

Data samples	Events in 914.1 days (final cut)
Astrophysical ν_τ CC	$(5.4 \pm 0.1) \times 10^{-1}$
Astrophysical ν_μ CC	$(1.8 \pm 0.1) \times 10^{-1}$
Astrophysical ν_e	$(6.0 \pm 1.7) \times 10^{-2}$
Atmospheric ν	$(3.2 \pm 1.4) \times 10^{-2}$
Atmospheric muons	$(7.5 \pm 5.8) \times 10^{-2}$

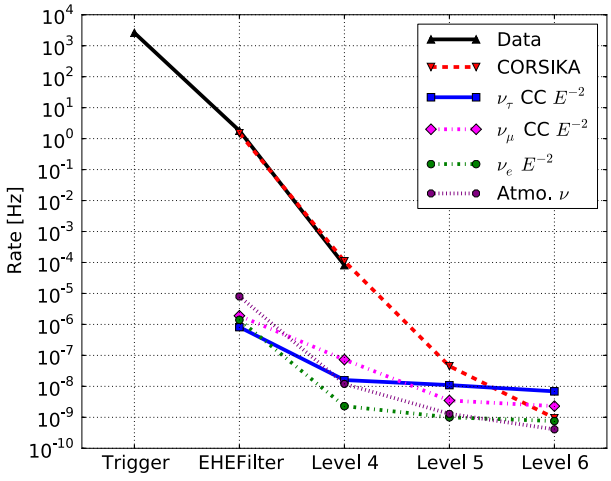

FIG. 5. Passing rate for signal (astrophysical ν_τ CC events in solid blue) and backgrounds (astrophysical ν_μ in dot-dashed magenta, astrophysical ν_e in dot-dashed green, atmospheric neutrinos in dotted purple, and atmospheric muons or CORSIKA in dashed red) as a function of cut level. Data shown here in solid black is 10% of the total data sample.

this double pulse method is around the PeV region, where the effective areas for ν_τ CC events are nearly an order of magnitude higher than that of ν_μ CC events. It is planned that events found at final cut level will be further investigated with segmented energy loss reconstruction algorithms [36] to acquire their energy loss profile and directionality. Event probabilities of ν_τ-like or not will also be computed based on likelihood methods.

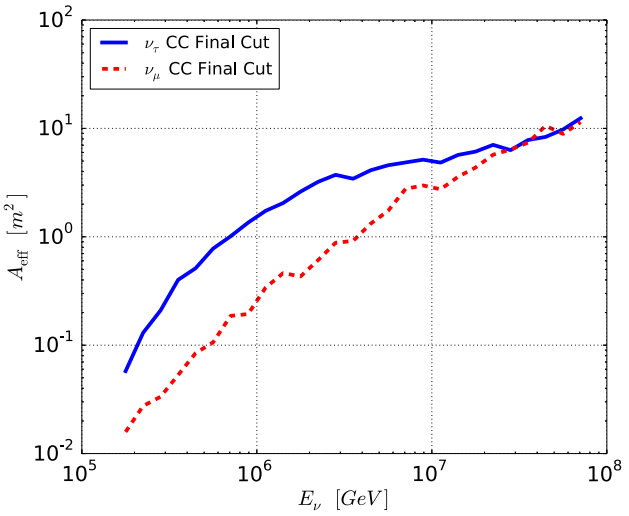

FIG. 6. Effective areas at final cut level as a function of primary neutrino energy. Only the middle 90% ν_τ energy range (214 TeV–72 PeV) is plotted. The dominant background for this analysis is due to astrophysical ν_μ CC events, so only ν_τ CC (solid blue) and ν_μ CC (dashed red) effective areas are shown. The plot demonstrates that the optimal energy window for the astrophysical ν_τ search using the double pulse waveform approach is from O(100) TeV to O(10) PeV. In particular, around PeV energies, effective areas for ν_τ CC events are about an order of magnitude higher than those for ν_μ CC events. Effective areas for ν_e (not shown) are 1–2 orders of magnitude below the effective areas for ν_τ CC, except at the Glashow resonance energy of 6.3 PeV [37].

IV. SYSTEMATIC UNCERTAINTIES

The sources of systematic uncertainty considered in this analysis are neutrino cross sections, anisotropy in the optical scattering in ice, uncertainty in the optical scattering and absorption lengths in ice, and DOM efficiency. The main sources of systematic uncertainty in the signal are summarized in Table II.

The neutrino cross sections used in this analysis are from the CTEQ5 model [38]. The CSMS model [39], which has updated parton distribution functions, predicts ∼5% fewer events compared to the CTEQ5 model.

An earlier study in IceCube attempting to reconstruct the double deposition of energy from a ν_τ CC event has found that the recently identified anisotropy in the optical scattering in ice [40] would modify the number of expected photons in some DOMs and hence could mimic a double cascade feature in the reconstructed energy segments [41]. A study based on simulations with and without this anisotropy found a 7% lower signal event rate prediction for the double pulse analysis when anisotropy was included. The effect is small at the waveform level due to the fact that the double pulse events usually occur within tens of meters of a DOM, which is within 1–2 scattering lengths in the ice.

The optical scattering length and absorption length were varied according to the uncertainty in the value of these parameters [33]. Increasing the absorption by the allowed uncertainty decreases the signal event rate by 4.9%, and decreasing the absorption and scattering increases the signal event rate by 8.1%.

Since the ν_τ double pulse events are very bright, uncertainty in the DOM efficiency does not play an important role. Simulation with the DOM efficiency set at $+10\%$ and -10% of the nominal values yielded a decrease of 1.6% in the signal event rate when decreasing the efficiency, and an increase of 6.7% in the signal event rate when increasing the efficiency.

Adding the various errors in quadrature, the total systematic uncertainty in the signal is about $\pm 10\%$.

The uncertainty in the atmospheric muon and neutrino background is dominated by statistical error, due to the

TABLE II. Source of systematic uncertainty in the signal.

Neutrino cross sections	-5%
Anisotropy in the optical scattering in ice	-7%
Optical scattering and absorption lengths in ice	$^{+8.1\%}_{-4.9\%}$
DOM efficiency	$^{+6.7\%}_{-1.6\%}$
Total	$^{+10.5\%}_{-10.0\%}$

fact that few simulated background events pass the cuts. The largest source of systematic error is uncertainty in the cosmic ray flux at high energies which contributes $+30\%/-50\%$ uncertainty to the atmospheric muon flux and $\pm 30\%$ uncertainty to the atmospheric neutrino flux [42].

V. RESULTS

Zero events were found after all cuts were applied. At level 5, before the containment cut, three events were found with each having one double pulse waveform, all of which occurred on strings at the edge of IceCube. These events are consistent with atmospheric muons interacting near the edge of the detector, producing a double pulse waveform in a cascadelike event but failing the subsequent containment cut at level 6. The observation of three events in 914.1 days of livetime matches the CORSIKA prediction at level 5 as discussed in Sec. III B. The events and their corresponding double pulse waveforms are shown in Figs. 7, 8, and 9.

Based on zero observed events, an integrated astrophysical ν_τ flux upper limit is set to be $E^2\Phi_{\nu_\tau} = 5.1 \times 10^{-8}$ GeV cm^{-2} sr^{-1} s^{-1}. A ν_τ flux differential upper limit in the energy range of 214 TeV to 72 PeV, which contains 90% of the predicted ν_τ CC events, is also extracted following the procedure that was employed in deriving quasidifferential upper limits from previous EHE cosmogenic neutrino searches in IceCube [42–44]. In this procedure, flux limits were computed for each energy decade with a sliding energy window of 0.1 decade, assuming a differential neutrino flux proportional to $1/E^2$ [45]. Since zero events were found, the 90% C.L.

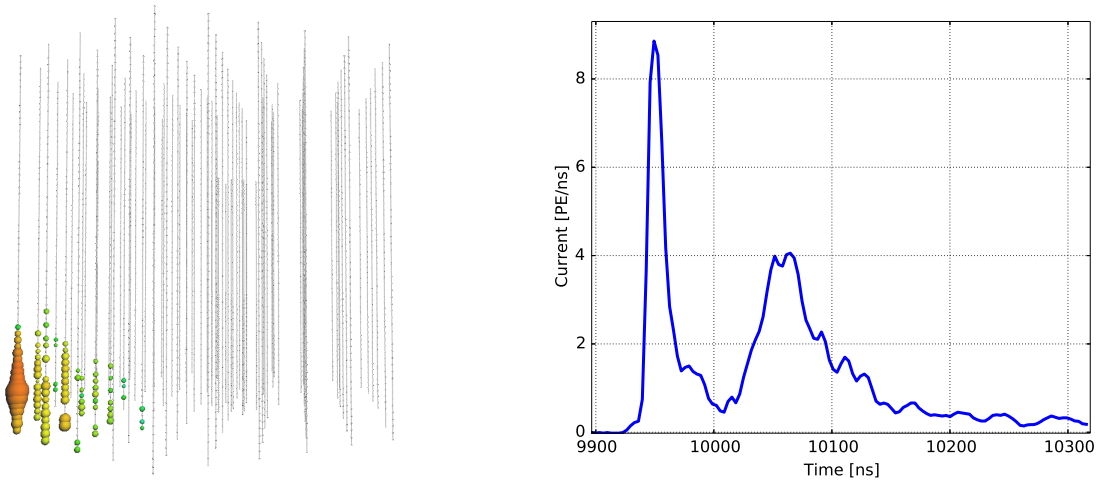

FIG. 7. Event 1 before level 6 containment cut with its corresponding double pulse waveform. This event occurred on May 30, 2011. The colored spheres indicate hit DOMs, with size indicating the amount of charge deposited on the sphere and color indicating time: red is earlier, blue is later.

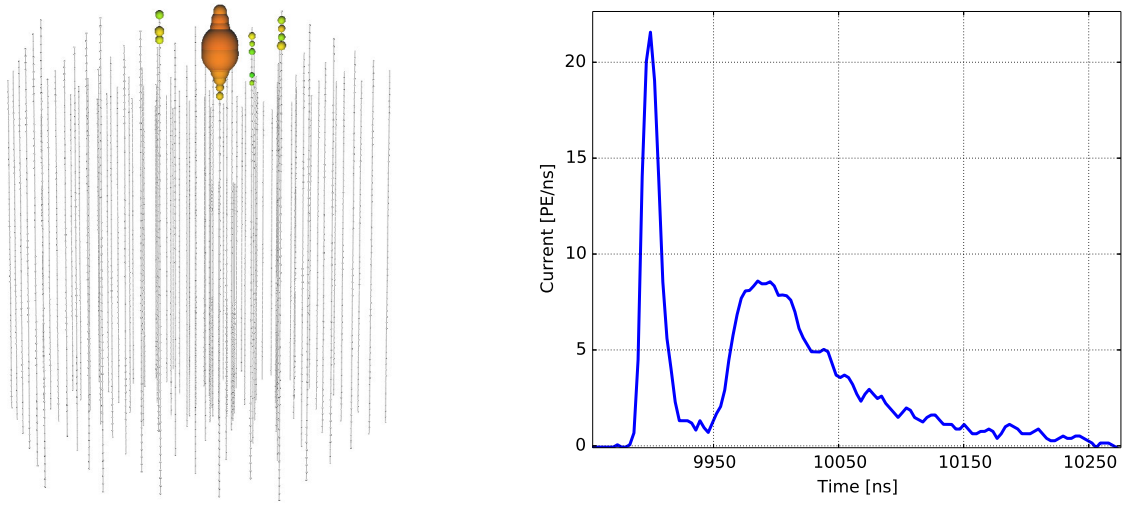

FIG. 8. Event 2 before level-6 containment cut with its corresponding double pulse waveform. This event occurred on November 27, 2011.

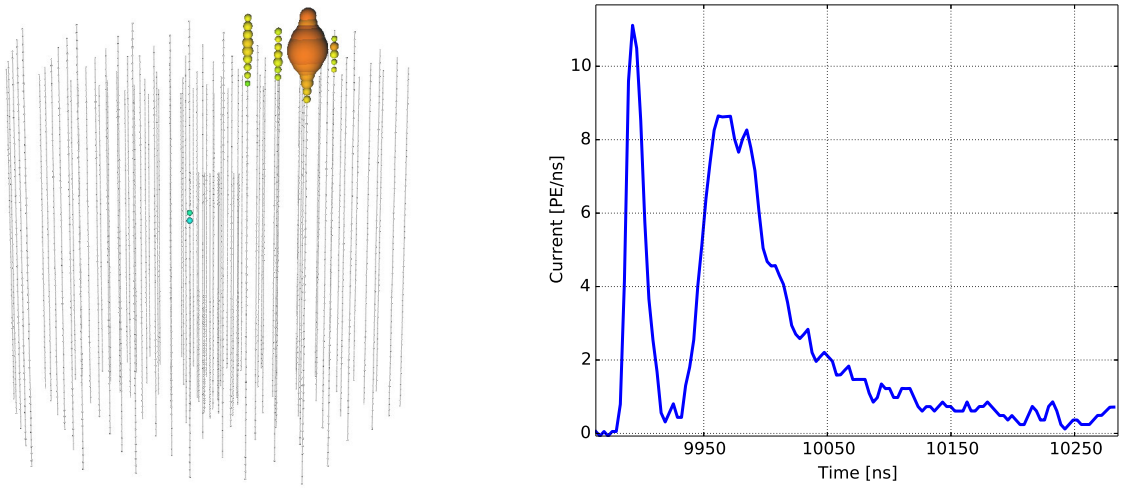

FIG. 9. Event 3 before level-6 containment cut with its corresponding double pulse waveform. This event occurred on August 28, 2012.

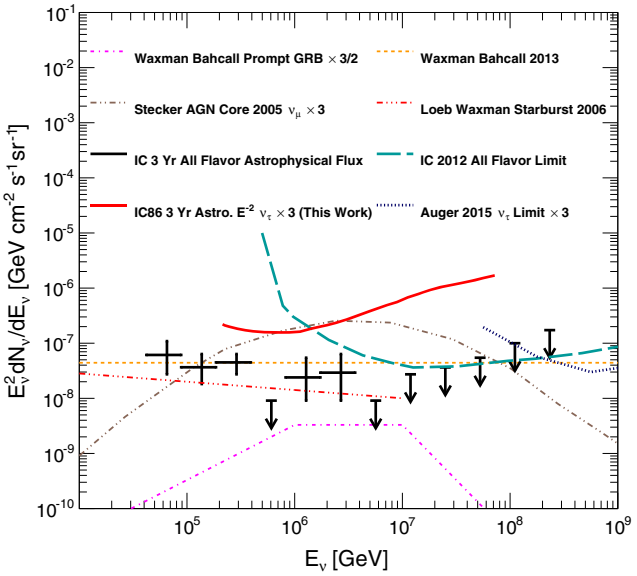

FIG. 10. Neutrino flux upper limits and models as a function of the primary neutrino energy. The thick red curve is the ν_τ differential upper limit derived from this analysis, including systematic and statistical errors. In computing the differential upper limit, values of the flux limit were calculated for each energy decade with a sliding energy window of 0.1 decade. The thick black error bars depict the all-flavor astrophysical neutrino flux observed by IceCube [2]. The thick dashed line is the differential upper limit derived from a search for extremely high energy events which has found the first two PeV cascade events in IceCube [42,47]. The blue dotted line is the Auger differential upper limit from ν_τ-induced air showers [27]. The orange dashed line is the Waxman-Bahcall upper bound which uses the UHECR flux to set a bound on astrophysical neutrino production [48]. The dash-dotted line (magenta) represents the prompt neutrino flux predicted from GRBs; prompt in this context means in time with the gamma rays [49]. The dash-dot-dot line (grey) indicates the neutrino flux predicted from the cores of active galaxies [50]. The thin dash-triple-dot line (red) shows the neutrino flux predicted from starburst galaxies, which are rich in supernovae [51].

event count limit in each energy decade is 2.44 based on the Feldman-Cousins approach [46]. The dominant sources of systematic error in this analysis are independent of energy. Therefore, all the sources of systematic and statistical error are incorporated in the limit calculation by uniform scaling of the effective area. The differential upper limit is plotted in Fig. 10.

VI. CONCLUSION

The double pulse search method is shown to be robust, with the observed background from cosmic-ray-induced muons matching prediction. The search is more sensitive to tau neutrinos between 214 TeV and 72 PeV than to any other flavor. Given the astrophysical neutrino flux observed by IceCube, fewer than one tau neutrino candidate event is expected in three years of IceCube data, and none are observed. A differential upper limit has been placed on the astrophysical tau neutrino flux, with an energy threshold 3 orders of magnitude lower than previous dedicated tau neutrino searches by cosmic ray air shower detectors. Searches for double bang events with well-separated cascades in IceCube are underway. Future extensions of IceCube such as the proposed IceCube-Gen2 detector [52] will have a factor of 5 to 10 times more sensitivity to astrophysical tau neutrinos than the current IceCube detector.

ACKNOWLEDGMENTS

We acknowledge the support from the following agencies: U.S. National Science Foundation-Office of Polar Programs, U.S. National Science Foundation-Physics Division, University of Wisconsin Alumni Research Foundation, the Grid Laboratory of Wisconsin (GLOW) grid infrastructure at the University of Wisconsin-Madison, the Open Science Grid (OSG) grid infrastructure; U.S.

Department of Energy, and National Energy Research Scientific Computing Center, the Louisiana Optical Network Initiative (LONI) grid computing resources; Natural Sciences and Engineering Research Council of Canada, WestGrid and Compute/Calcul Canada; Swedish Research Council, Swedish Polar Research Secretariat, Swedish National Infrastructure for Computing (SNIC), and Knut and Alice Wallenberg Foundation, Sweden; German Ministry for Education and Research (BMBF), Deutsche Forschungsgemeinschaft (DFG), Helmholtz Alliance for Astroparticle Physics (HAP), Research Department of Plasmas with Complex Interactions (Bochum), Germany; Fund for Scientific Research (FNRS-FWO), FWO Odysseus program, Flanders Institute to encourage scientific and technological research in industry (IWT), Belgian Federal Science Policy Office (Belspo); University of Oxford, United Kingdom; Marsden Fund, New Zealand; Australian Research Council; Japan Society for Promotion of Science (JSPS); the Swiss National Science Foundation (SNSF), Switzerland; National Research Foundation of Korea (NRF); Danish National Research Foundation, Denmark (DNRF).

[1] M. Aartsen *et al.* (IceCube Collaboration), Science **342**, 1242856 (2013).
[2] M. Aartsen *et al.*, Phys. Rev. Lett. **113**, 101101 (2014).
[3] J. G. Learned and S. Pakvasa, Astropart. Phys. **3**, 267 (1995).
[4] L. A. Anchordoqui, H. Goldberg, F. Halzen, and T. J. Weiler, Phys. Lett. B **593**, 42 (2004).
[5] J. P. Rachen and P. Mészáros, Phys. Rev. D **58**, 123005 (1998).
[6] T. Kashti and E. Waxman, Phys. Rev. Lett. **95**, 181101 (2005).
[7] M. Kachelrieß and R. Tomàs, Phys. Rev. D **74**, 063009 (2006).
[8] P. Lipari, M. Lusignoli, and D. Meloni, Phys. Rev. D **75**, 123005 (2007).
[9] S. R. Klein, R. E. Mikkelsen, and J. B. Tjus, Astrophys. J. **779**, 106 (2013).
[10] L. A. Anchordoqui *et al.*, J. High Energy Astrophys. **1–2**, 1 (2014).
[11] M. G. Aartsen *et al.* (IceCube Collaboration), Phys. Rev. Lett. **114**, 171102 (2015).
[12] M. G. Aartsen *et al.* (IceCube Collaboration), Astrophys. J. **809**, 98 (2015).
[13] F. Halzen and D. Saltzberg, Phys. Rev. Lett. **81**, 4305 (1998).
[14] R. Enberg, M. H. Reno, and I. Sarcevic, Phys. Rev. D **78**, 043005 (2008).
[15] J. F. Beacom, N. F. Bell, D. Hooper, S. Pakvasa, and T. J. Weiler, Phys. Rev. Lett. **90**, 181301 (2003).
[16] P. Baerwald, M. Bustamante, and W. Winter, J. Cosmol. Astropart. Phys. 10 (2012) 020.
[17] H. Athar, M. Jeżabek, and O. Yasuda, Phys. Rev. D **62**, 103007 (2000).
[18] J. F. Beacom, N. F. Bell, D. Hooper, J. G. Learned, S. Pakvasa, and T. J. Weiler, Phys. Rev. Lett. **92**, 011101 (2004).
[19] A. Esmaili, Phys. Rev. D **81**, 013006 (2010).
[20] D. Hooper, D. Morgan, and E. Winstanley, Phys. Rev. D **72**, 065009 (2005).
[21] L. A. Anchordoqui, H. Goldberg, M. C. Gonzalez-Garcia, F. Halzen, D. Hooper, S. Sarkar, and T. J. Weiler, Phys. Rev. D **72**, 065019 (2005).
[22] C. A. Argüelles, T. Katori, and J. Salvado, Phys. Rev. Lett. **115**, 161303 (2015).
[23] M. Bustamante, J. F. Beacom, and W. Winter, Phys. Rev. Lett. **115**, 161302 (2015).
[24] A. Palladino and F. Vissani, Eur. Phys. J. C **75**, 433 (2015).
[25] R. Abbasi *et al.* (IceCube Collaboration), Phys. Rev. D **86**, 022005 (2012).
[26] D. Cowen *et al.* (IceCube Collaboration), in *Journal of Physics: Conference Series*, Vol. 60 (IOP Publishing, London, 2007), p. 227.
[27] A. Aab *et al.* (Pierre Auger), Phys. Rev. D **91**, 092008 (2015).
[28] A. Achterberg *et al.*, Astropart. Phys. **26**, 155 (2006).
[29] R. Abbasi *et al.* (IceCube Collaboration), Nucl. Instrum. Methods, Sect. A **618**, 139 (2010).
[30] R. Abbasi *et al.* (IceCube Collaboration), Nucl. Instrum. Methods, Sect. A **601**, 294 (2009).
[31] D. Heck, G. Schatz, T. Thouw, J. Knapp, and J. Capdevielle, Tech. Rep. FZKA **6019** (1998).
[32] A. Gazizov and M. Kowalski, Comput. Phys. Commun. **172**, 203 (2005).
[33] M. Aartsen *et al.* (IceCube Collaboration), Nucl. Instrum. Methods, Sect. A **711**, 73 (2013).
[34] M. Honda, T. Kajita, K. Kasahara, S. Midorikawa, and T. Sanuki, Phys. Rev. D **75**, 043006 (2007).
[35] T. K. Gaisser, Astropart. Phys. **35**, 801 (2012).
[36] M. G. Aartsen *et al.* (IceCube Collaboration), JINST **9**, P03009 (2014).
[37] S. L. Glashow, Phys. Rev. **118**, 316 (1960).
[38] H. Lai, J. Huston, S. Kuhlmann, J. Morfin, F. Olness, J. Owens, J. Pumplin, and W. Tung, Eur. Phys. J. C **12**, 375 (2000).
[39] A. Cooper-Sarkar, P. Mertsch, and S. Sarkar, J. High Energy Phys. 08 (2011) 042.
[40] M. Aartsen *et al.* (IceCube Collaboration), arXiv:1309.7010.
[41] P. Hallen, On the Measurement of High-Energy Tau Neutrinos with IceCube, Master's thesis (RWTH Aachen, 2013).
[42] M. Aartsen *et al.* (IceCube Collaboration), Phys. Rev. D **88**, 112008 (2013).
[43] R. Abbasi *et al.* (IceCube Collaboration), Phys. Rev. D **82**, 072003 (2010).

[44] R. Abbasi *et al.* (IceCube Collaboration), Phys. Rev. D **83**, 092003 (2011).
[45] I. Kravchenko *et al.* (RICE Collaboration), Phys. Rev. D **73**, 082002 (2006).
[46] G. J. Feldman and R. D. Cousins, Phys. Rev. D **57**, 3873 (1998).
[47] M. Aartsen *et al.* (IceCube Collaboration), Phys. Rev. Lett. **111**, 021103 (2013).
[48] E. Waxman, arXiv:1312.0558.
[49] E. Waxman and J. N. Bahcall, Phys. Rev. Lett. **78**, 2292 (1997).
[50] F. W. Stecker, Phys. Rev. D **72**, 107301 (2005).
[51] A. Loeb and E. Waxman, J. Cosmol. Astropart. Phys. 05 (2006) 003.
[52] M. Aartsen *et al.* (IceCube Collaboration), arXiv: 1412.5106.